

RESEARCH LETTER

10.1002/2015GL063834

Key Points:

- Plasticity reduces the dependence of radius of curvature on slab thickness
- Plasticity introduces dependence of curvature on upper plate thickness
- Natural subduction zones exhibit systematics observed in plastic slabs models

Supporting Information:

- Text S1 and Captions of Figures S1–S5
- Figure S1
- Figure S2
- Figure S3
- Figure S4
- Figure S5

Correspondence to:

A. F. Holt,
adamholt@usc.edu

Citation:

Holt, A. F., B. A. Buffett, and T. W. Becker (2015), Overriding plate thickness control on subducting plate curvature, *Geophys. Res. Lett.*, *42*, 3802–3810, doi:10.1002/2015GL063834.

Received 11 MAR 2015

Accepted 30 APR 2015

Accepted article online 6 MAY 2015

Published online 22 MAY 2015

Overriding plate thickness control on subducting plate curvature

Adam F. Holt¹, Bruce A. Buffett², and Thorsten W. Becker¹

¹Department of Earth Sciences, University of Southern California, Los Angeles, California, USA, ²Department of Earth and Planetary Science, University of California, Berkeley, California, USA

Abstract Subducting plate (SP) curvature exerts a key control on the amount of bending dissipation associated with subduction, and the magnitude of the subduction-resisting bending force. However, the factors controlling the development of SP curvature are not well understood. We use numerical models to quantify the role of SP rheology on the minimum radius of curvature, R_{\min} . We find that R_{\min} depends strongly on the SP thickness when the rheology is viscous. This dependence is substantially reduced when the SP behaves plastically, in line with the lack of correlation between R_{\min} and SP thickness on Earth. In contrast, plasticity leads to a strong positive correlation between R_{\min} and the overriding plate (OP) thickness. Using an analysis of R_{\min} versus OP thickness, we show that such a positive correlation exists on Earth. This suggests that OP structure, in conjunction with SP plasticity, is crucial in generating slab curvature systematics on Earth.

1. Introduction

Subducting slabs have long been recognized as the major driver of plate motions on Earth [Forsyth and Uyeda, 1975]. The change of gravitational potential energy due to lithospheric plates sinking into the mantle is balanced by viscous dissipation in both the plates and the surrounding mantle. The curvature of the subducting plate (SP) at the trench exerts a key control on the amount of dissipation due to plate bending, and the size of the subduction-resisting bending force [e.g., Conrad and Hager, 1999; Becker et al., 1999; Buffett, 2006; Wu et al., 2008; Ribe, 2010].

Significant attention has been given to the influence of SP parameters on slab curvature: Assuming that bending dissipates a constant proportion of the work done by sinking slabs, a positive scaling is expected between SP thickness and radius of curvature [Buffett, 2006; Buffett and Heuret, 2011]. Such an increase in SP curvature for thick SPs is indeed observed in laboratory [Bellahsen et al., 2005; Schellart, 2009; Irvine and Schellart, 2012] and numerical [Capitanio et al., 2009] experiments with viscous slabs. However, a positive correlation between SP age, which controls plate thickness, and R_{\min} , estimated from earthquake hypocenter distributions, appears to be absent on Earth [Buffett and Heuret, 2011; Fourel et al., 2014]. It has been suggested that a plastic rheology component, in which the SP hinge viscosity is reduced due to stresses induced by the SP's negative buoyancy, could explain the discrepancy between the radius of curvature systematics observed on Earth, and that predicted for a viscous plate [Buffett and Heuret, 2011; Buffett and Becker, 2012]. Such plastic weakening of the SP bending region, e.g., in the form of deep crustal faulting, is expected to occur on Earth [e.g., Ranero et al., 2003, 2005], driven by the bending stresses of the negatively buoyant SP [e.g., Billen and Gurnis, 2001]. We therefore consider how the dependence of R_{\min} on SP thickness is modified for viscoplastic SPs, relative to the isoviscous SPs typically considered in such studies.

In addition to the physical properties of the SP, recent numerical experiments have shown that overriding plate (OP) structure can exert a strong control on SP dynamics/morphology [e.g., Yamato et al., 2009; Sharples et al., 2014; Garel et al., 2014]. Particularly, thick OPs result in SPs with large mantle-scale dips. However, the possibility that OP structure exerts a control on R_{\min} , and so slab bending remains unexplored as experiments investigating slab curvature have so far been constrained to single-plate studies, thus neglecting the possible role of the OP. For plastic plates, Buffett and Becker [2012] showed that the bending moment may saturate during subduction, because hinge stresses can be limited by the plastic yield stress. A consequence of this saturation is that the bending stresses may not be large enough to balance the opposing gravitational torque [Ribe, 2010; Buffett and Becker, 2012]. Thus, additional forces associated with the OP or plate interface/weak zone have been hypothesized to play a role [Buffett and Becker, 2012] and may exert a

control on the development of slab curvature. Using the dynamically self-consistent, two plate models of *Holt et al.* [2015], we therefore investigate the effect of OP thickness, h_{OP} , on the curvature of the SP (R_{min}). In addition to moving toward more Earth-like numerical models, incorporating interactions between the two plates allows us to directly investigate how SP rheology, in conjunction with OP structure, affects the dynamics of the subducting slab.

Lastly, after characterizing the dependence of slab curvature on lithospheric plate thickness for various simple slab rheologies, we compare the model systematics to those derived from slab curvature estimates on Earth. While previous compilations of subduction zone parameters suggest a correlation between slab dip and OP velocity and/or deformation regime [e.g., *Lallemand and Heuret*, 2005; *Heuret et al.*, 2007], a potential OP thickness control on slab curvature has not been investigated. We use the R_{min} estimates of *Buffett and Heuret* [2011] and the lithospheric thickness estimates of *Bird et al.* [2008] to first verify the lack of a correlation between R_{min} and SP thickness, and then probe subduction zones on Earth for a potential correlation between R_{min} and OP thickness.

2. Numerical Method and Model Setup

We use the finite element code CitcomCU [*Moresi and Gurnis*, 1996; *Zhong*, 2006] to model subduction in a Cartesian domain. CitcomCU solves the equations governing convection in an incompressible viscous fluid (Boussinesq approximation) with negligible inertia. The domain size is 7920 km \times 1320 km \times 13.2 km (i.e., the computation is effectively 2-D), and all boundaries are mechanically free slip. The initial subducting and overriding plate lengths are 4500 km and 2400 km, respectively. Thermally, the upper boundary has a constant temperature of 273 K, while the base and sides have zero heat flux. In order to target first-order dynamics, we use a simple subduction setup, both mechanically and rheologically. The lithosphere-asthenosphere temperature contrast is set to 1200 K. Because we use thick, constant temperature lithospheric plates, as opposed to a half-space cooling profiles, we use a reduced thermal expansivity, of $1.25 \times 10^{-5} \text{ K}^{-1}$, to give a reasonable bulk density contrast of 50 kg/m³. The sublithospheric mantle has a reference viscosity of 10^{20} Pa s and density of 3300 kg/m³. With a thermal diffusivity, κ , of $10^{-6} \text{ m}^2/\text{s}$, this corresponds to a Rayleigh number of 1.13×10^7 .

In the constant viscosity SP models (“viscous” models), lithospheric plates are a factor of 500 more viscous than the sublithospheric mantle. Viscosity is defined according to *Frank-Kamenetskii* [1969], using a high-temperature dependence ($E = 10$) and is limited by a maximum cutoff ($500\eta_0$),

$$\eta_N = \min(\eta_0 \exp(E(1 - T)), 500\eta_0), \quad (1)$$

where T is the nondimensional temperature. In the viscoplastic SP models, an additional plastic viscosity is added to the rheological formulation. The effective viscosity, η_{eff} , is then taken as the minimum of η_N and the plastic viscosity, which limits the allowable stress to the value of the yield stress, τ_y [e.g., *Schott and Schmeling*, 1998; *Enns et al.*, 2005]:

$$\eta_{eff} = \min\left(\eta_N, \frac{\tau_{yield}}{2\dot{\epsilon}_{ij}}\right), \quad (2)$$

where $\dot{\epsilon}_{ij} = \sqrt{\dot{\epsilon}_{ij}\dot{\epsilon}_{ij}/2}$ is the second invariant of the deviatoric strain rate (Einstein summation convention). To focus on the role of the SP rheology, we confine plastic yielding to within the SP. This ensures that the strength of the OP is constant throughout models and so removes the possibility that differential rates of OP deformation contribute to the observed curvature variations. For simplicity, we consider a constant τ_y . In order to capture varying degrees of plastic yielding, we test three τ_y values of 50, 75, and 100 MPa. As in many other subduction modeling studies [e.g., *Schott and Schmeling*, 1998; *Enns et al.*, 2005; *Di Giuseppe et al.*, 2008], our τ_y values are significantly lower than experimental estimates of the depth-averaged yield stress in oceanic lithosphere (300 MPa) [*Mei et al.*, 2010]. While this discrepancy remains enigmatic, in the current work we do not aim to replicate the exact mechanics of subduction on Earth but probe potential mechanisms responsible for first-order trends observed. Our τ_y values have been chosen empirically, in order to be high enough to prevent the SP hinge from completely weakening and low enough to place a significant proportion of the hinge in the plastic regime.

Subduction is initiated by allowing the SP to extend below the OP to a depth of 200 km with a radius of curvature (R_{init}) of 250 km. We examine how this initial condition affects the dynamics observed by testing

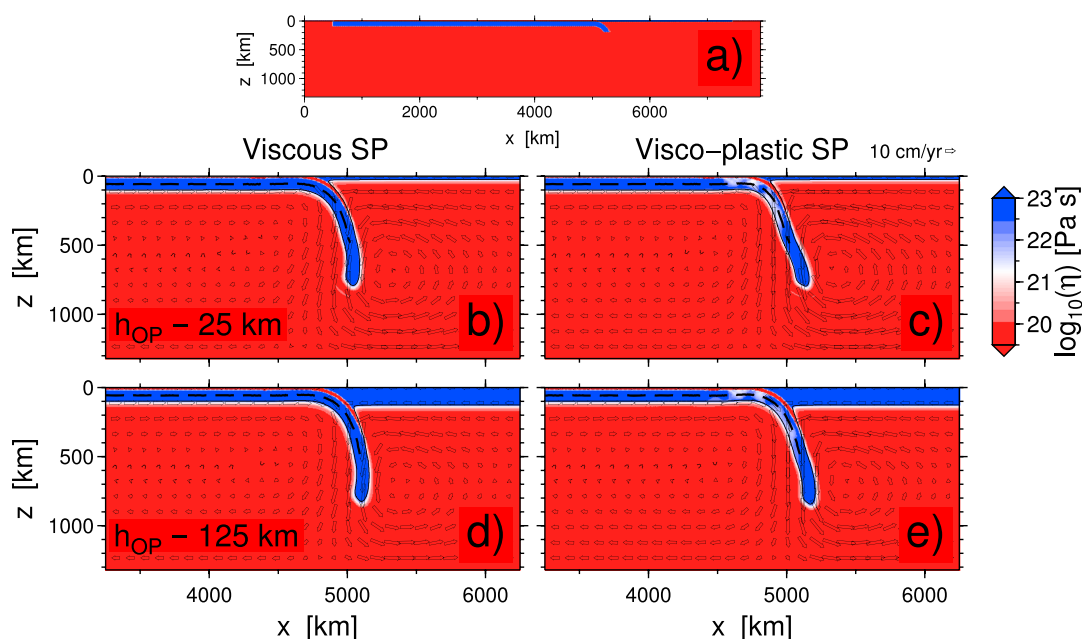


Figure 1. Model viscosity field of (a) initial model setup for viscous case with $h_{SP} = 100$ km and $h_{OP} = 25$ km and (b–e) at evolved time steps for a selection of models with variable h_{OP} . Figures 1b and 1d show models with a viscous subducting plate rheology (Figure 1b: $h_{OP} = 25$ km, Figure 1d: 125 km), and Figures 1c and 1e show models with a viscoplastic subducting plate rheology with $\tau_y = 75$ MPa (Figure 1c: $h_{OP} = 25$ km, Figure 1e: 125 km). In all models shown, $h_{SP} = 100$ km. The subducting plate centerlines used to compute R_{min} are overlain in black.

other values of R_{init} (200 km and 300 km). To facilitate decoupling of the SP from the OP, we insert a 15 km thick, weak ($0.5\eta_{mant}$) crustal layer within the SP [e.g., Běhounková and Čížková, 2008; Stegman et al., 2010]. More details about the implementation of this compositional crust, and resolution tests of similar models are described in Holt et al. [2015]. Finite element dimensions vary from 2.5 km in the upper 330 km of the domain to 7.5 km elsewhere. In order to investigate the dependence of slab curvature on the SP and OP thicknesses (h_{SP} , h_{OP}), we vary h_{SP} between 75 and 125 km (with $h_{OP} = 50$ km), and h_{OP} between 25 and 125 km (with $h_{SP} = 100$ km).

To compute the radius of curvature, we track the location of the subducting plate centerline, i.e., halfway between the top and base of the lithosphere (Figure 1). This is done by placing passive tracers at the, initially horizontal, plate center and allowing them to advect in the induced flow field. The minimum radius of curvature, R_{min} , is then computed by fitting cubic splines to the SP centerline, according to the methodology of Buffett and Heuret [2011]. While R_{min} is strongly time dependent, we choose to compute the typical R_{min} at an equivalent slab tip depth of 760 km in each of the models. We do this by linearly interpolating R_{min} to this depth using the two adjacent numerical time steps, as illustrated in Figure S1 in the supporting information. This depth corresponds to halfway between the initial slab depth (200 km) and the base of the model (1320 km) and gives the bending region enough time to evolve from the geometry initially imposed while being far enough from the base to not be significantly affected by the bottom of the box. We additionally examine the temporal evolution of R_{min} in the supporting information (Figure S1).

3. Plate Thickness Control on Radius of Curvature

Initially, we focus on the effect of the subducting plate thickness, h_{SP} , on radius of curvature for a constant overriding plate thickness, h_{OP} , of 50 km (Figure 2b). For these experiments, the OP is thinner than the SP, in order to focus on the dynamics of the SP. As observed previously for single-plate models [Bellahsen et al., 2005; Schellart, 2009; Irvine and Schellart, 2012], the radius of curvature (R_{min}) for viscous SPs increases with increasing h_{SP} . R_{min} increases from 185 to 280 km when h_{SP} is increased from 75 to 125 km (Figure 2b). The dependence is near linear with an average slope, computed from the two end points, of 1.9. In detail, it appears that the relationship is slightly nonlinear with a power law exponent, computed from a linear regression of a log-log plot, of 0.81 (Figure S3a).

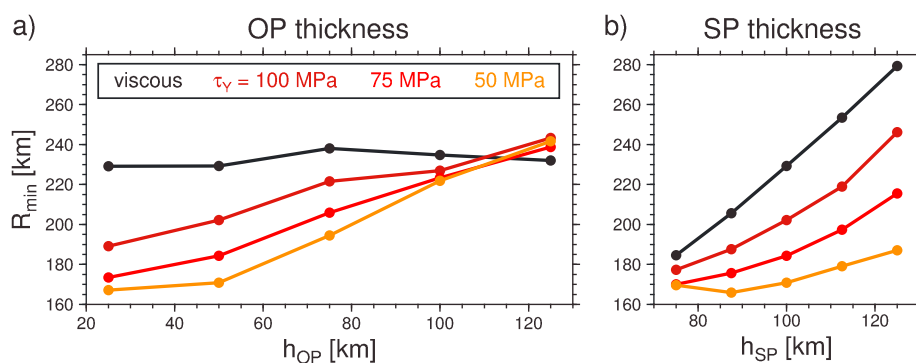


Figure 2. Dependence of R_{\min} on (a) h_{OP} and (b) h_{SP} . R_{\min} is computed at an equivalent slab tip in each model ($z_{\text{slab}} = 760$ km). For the models with variable h_{OP} , $h_{SP} = 100$ km, and for the models with variable h_{SP} , $h_{OP} = 50$ km. All models have equivalent initial curvature, $R_{\text{init}} = 250$ km.

The strength of the h_{SP} control on R_{\min} significantly weakens with the addition of a plastic viscosity component in the SP, and the dependence becomes much more strongly nonlinear (Figure 2b). For a yield stress of 100 MPa, R_{\min} increases by 69 km when increasing h_{SP} from 75 to 125 km. This change in R_{\min} is $\sim 70\%$ of that observed in the viscous plate models. Reducing τ_y , which increases the area of the bending region deforming plastically, reduces the strength of this positive trend further still. In the models with τ_y of 50 MPa, R_{\min} increases by only 17 km, or $\sim 20\%$ of the change for the viscous plates. In addition, for all values of h_{SP} , viscoplastic SPs have reduced R_{\min} relative to the equivalent viscous SP models.

We next examine the control of the overriding plate thickness, h_{OP} , on R_{\min} , for a constant $h_{SP} = 100$ km (Figure 2a). The radius of curvature of viscous SPs is found to be largely independent of h_{OP} , with a relatively constant R_{\min} of ~ 230 km for a wide range of h_{OP} , from 25 to 125 km. Conversely, SPs with a plastic viscosity component exhibit a strong positive correlation between R_{\min} and h_{OP} . The trends are approximately linear, albeit much less uniform than the trend between h_{SP} and R_{\min} for viscous SPs (Figure 2b), and so we use the slope computed from the end points at $R(h_{OP} = 25$ km) and $R(h_{OP} = 125$ km) to compare the strength of the relationship for variable yield stresses. For τ_y of 50, 75, and 100 MPa, the slope is 1.5, 1.3, and 1.1, respectively. Therefore, the radius of curvature has a stronger dependence on h_{OP} when the size of the region of plastic failure increases. As observed when examining h_{SP} , R_{\min} is generally reduced for viscoplastic SPs relative to the equivalent viscous models. In addition, for the thickest overriding plates, R_{\min} converges to a relatively constant ~ 240 km.

In order to test whether the positive correlation between R_{\min} and h_{OP} is representative of the entire model runs, we additionally examine the time dependence of R_{\min} in the supporting information. In Figure S1, R_{\min} is plotted as a function of slab tip depth (z_{slab}) for both viscous models and the intermediate yield stress viscoplastic models ($\tau_y = 75$ MPa) with variable h_{OP} . As observed previously [e.g., Becker *et al.*, 1999; Capitanio *et al.*, 2007; Irvine and Schellart, 2012], R_{\min} is strongly time dependent. However, the positive correlation between R_{\min} and h_{OP} for the viscoplastic models is prevalent throughout the majority of the model run, while the R_{\min} trajectory clearly shows no such dependence for the viscous SP models. Only during the initial period, when the SP is dynamically adjusting away from the morphology initially imposed (200 km $< z_{\text{slab}} < 550$ km), are these trends less developed. In addition, as the slab tip gets close to the base of the box ($z = 1320$ km), R_{\min} increases as the slab dip reduces. We therefore consider the trends shown in Figure 2 to be representative of the free-sinking phase of the dynamic models.

4. Correlations on Earth

Following the numerical modeling observations that a plastic subducting plate rheology gives rise to a positive correlation between R_{\min} and h_{OP} and a reduced correlation between R_{\min} and h_{SP} , we now turn our attention to subduction zones on Earth to test this hypothesis. We use the R_{\min} estimates of Buffett and Heuret [2011], computed from spline fits to 133 earthquake hypocenter profiles along 12 major subduction zone systems. Additionally, as in Lallemand and Heuret [2005], we remove 12 anomalous SP profiles that contain ridges, plateaus, or continental lithosphere. However, our findings do not depend on this selection (see below).

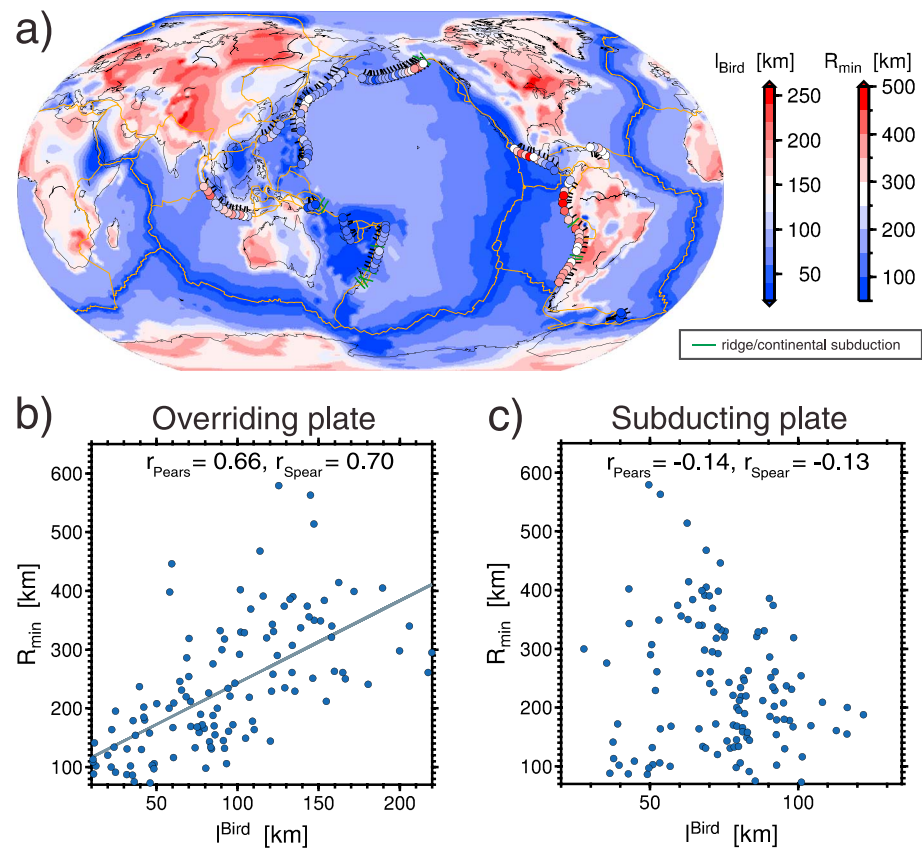


Figure 3. Correlation between radius of curvature, R_{\min} , and lithospheric thickness extracted from the *Bird et al.* [2008] model. (a) Lithospheric thickness map overlain by R_{\min} estimates (points) located at the profile locations used for the spline fit [Buffett and Heuret, 2011]. Green profiles indicate anomalous subduction segments omitted from the correlations. (b) Scatterplot of R_{\min} against the corresponding overriding plate thickness, extracted from the lithospheric thickness map at a position denoted by the onboard extent of the black ticks (i.e., 500 km away from the trench). Grey line shows the linear regression fit, and the legend specifies linear (Pearson) and Spearman rank correlation values. (c) Scatterplot of R_{\min} against the corresponding subducting plate thickness, extracted from the lithospheric thickness map at a position denoted by the outboard extent of the black ticks (i.e., 250 km away from trench).

We derive h_{OP} estimates from the *Bird et al.* [2008] model of lithospheric thickness which is itself derived from the S20RTS model of global shear velocity variations [Ritsema et al., 2004], and other geophysical constraints. The h_{OP} data point is picked at 500 km inboard of the subduction zone trench along the trench-perpendicular azimuth of the profiles used to compute R_{\min} (Figure 3a). We observe a positive correlation between R_{\min} and h_{OP} (Figure 3b), as observed for viscoplastic SPs in the numerical modeling (Figure 2a). We compute a linear (Pearson) correlation coefficient of 0.66 and a Spearman's rank correlation coefficient of 0.70 (Figure 3b). While such correlation coefficient values are encouraging, there is undoubtedly strong uncertainty in these data sets, particularly the tomographically derived h_{OP} estimates. Also, the appropriate distance from the trench to pick the overriding plate thickness likely varies between different subduction zone segments, due to the wedge geometry and lateral extent of overriding plate deformation. However, using a constant trench-OP distance appears appropriate for examining global trends. While we find that 500 km gives the highest correlation coefficients, we observe positive correlation coefficients, ranging from 0.52 to 0.69 for distances of 250 and 750 km (Figure S2). In addition, using the full Buffett and Heuret [2011] data set (i.e., not removing profiles containing ridges/continental material) reduces both the linear (Pearson) and Spearman's rank correlation coefficients by only 0.03 (Figure S2).

Inspecting these data sets geographically it is apparent that this positive correlation, on a global scale, is largely due to SPs subducting beneath thick continental lithosphere in the Eastern Pacific having large R_{\min} (typically $250 \text{ km} < R_{\min} < 500 \text{ km}$) and SPs subducting beneath thinner, oceanic OPs in the Western Pacific

having smaller R_{\min} (typically $75 \text{ km} < R_{\min} < 250 \text{ km}$) (Figure 3a). A more local region which appears to follow the hypothesized positive $R_{\min} - h_{\text{OP}}$ correlation appears is Central America/Mexico. In Central America, R_{\min} appears to be locally reduced in the region of low h_{OP} , relative to Mexico where a thicker OP gives rise to greater R_{\min} . In contrast, the subducting plate is younger/thinner in the northern portion of the Cocos plate where R_{\min} is greatest. It therefore appears that, at least along this subduction zone, the OP mechanical properties dominate over those of the SP in controlling slab curvature. There are, however, subduction zones within which this positive correlation between h_{OP} and R_{\min} does not appear to be present. Most striking are some of the profiles in the Sunda-Banda arc, where SPs with large R_{\min} of 300–400 km subduct beneath OPs that appear to be relatively thin (~50–125 km). Despite removing profiles with obvious SP ridges/plateaus, there are likely still significant buoyancy anomalies in the subducting plate due to the highly heterogeneous nature of this arc [e.g., *McBride and Karig*, 1987]. In such locations, and other regions with significant SP buoyancy heterogeneity, local R_{\min} variation is likely dominated by SP structure. However, on a global scale it appears that OP structure is playing a key role in dictating SP curvature. In addition to OP thickness, the density structure of the OP may also impact SP curvature by controlling the lithostatic pressure gradient exerted across the plate interface. The Banda-Sunda arc is a candidate for such an effect, as the OP transitions from continental in the west to oceanic in the east.

Lastly, we verify that there is indeed a poor correlation between R_{\min} and subducting plate thickness (h_{SP}). We extract h_{SP} from the same lithospheric thickness map, at a distance of 250 km outboard of the trench (Figure 3c). As reported in previous work [*Buffett and Heuret*, 2011], we compute very low, and negative, correlation coefficient values of -0.14 (Pearson) and -0.13 (Spearman). The lack of a positive correlation between R_{\min} and h_{SP} is incompatible with the systematics observed for purely viscous SPs in the numerical models (Figure 2b) and provides further support for the importance of SP plasticity.

5. Discussion

Previous modeling studies have investigated how h_{SP} affects R_{\min} for isoviscous slabs [e.g., *Bellahsen et al.*, 2005; *Schellart*, 2009; *Irvine and Schellart*, 2012]. However, the derived scaling relationships appear to be absent on Earth [*Buffett and Heuret*, 2011; *Fourel et al.*, 2014]. This led *Buffett and Heuret* [2011] to speculate that plasticity may be important in producing the curvature systematics observed on Earth. In addition to examining how plasticity can modify the curvature systematics, we consider the possible role of overriding plate structure, which has thus far remained unexplored. We are able to investigate this interaction because our numerical models self-consistently couple the dynamics of the two plates, without imposing kinematic constraints.

However, we do simplify many aspects of the physical system. Most notably, we adopt a simplified lithospheric viscosity structure, thus neglecting the layered rheological structure inferred from experimental work [e.g., *Goetze and Evans*, 1979; *Karato and Wu*, 1993; *Kohlstedt et al.*, 1995], and omit density/viscosity contrasts associated with midmantle phase transitions. In addition, our simulations are 2-D and so we neglect both the roles of toroidal flow [e.g., *Funiciello et al.*, 2003; *Kincaid and Griffiths*, 2003] and dissipation due to lithospheric bending in the third dimension. Lastly, we do not include a deformable free surface, instead prescribing a free-slip upper boundary. Despite such simplifications, our numerical setup allows us to identify the first-order effects of OP structure, and SP hinge weakening, on slab curvature, which is a crucial step prior to moving on to more Earth-like simulations.

5.1. Curvature as a Function of SP Thickness

A key observation in the numerical models is that R_{\min} increases with h_{SP} for viscous SPs (Figure 2b). While this relationship has not been explored in models with a coupled OP, previous single-plate studies also find that a thicker, isoviscous SP results in a greater R_{\min} [*Bellahsen et al.*, 2005; *Schellart*, 2009; *Irvine and Schellart*, 2012]. A linear dependence of R_{\min} on h_{SP} is reported in the studies aforementioned. The linear $h_{\text{SP}}-R_{\min}$ trends have variable slopes, presumably due to variable SP rheologies/strengths (*Irvine and Schellart* [2012]: 2.8 and *Bellahsen et al.* [2005]: 4.5), relative to the reduced average slope of 1.9 found here. While the trend observed here is near linear, the power law exponent deviates slightly from 1, with a value of 0.81 (Figure S3a). To first order, this basic positive trend can be understood by assuming that SP bending dissipates a constant proportion of the buoyancy flux energy source [e.g., *Conrad and Hager*, 1999]. A proportionality between

the buoyancy flux (left-hand side) and a thin-sheet approximation of the bending dissipation (right-hand side) gives

$$\Delta\rho gh_{sp}Dv_{sp} \propto \left(\frac{h_{sp}}{R_{min}}\right)^3 \eta' v_{sp}^2, \quad (3)$$

where $\Delta\rho$ is the slab mantle density contrast, g the acceleration due to gravity, D the slab depth, v_{sp} the subducting plate velocity, and η' the slab mantle viscosity ratio. Rearranging for R_{min} yields

$$R_{min} \propto h_{sp}^{2/3} v_{sp}^{1/3}. \quad (4)$$

We find that v_{sp} has a power law dependence on h_{sp} , with a power law exponent of 0.38 (Figure S3b). Substituting this dependence in for v_{sp} into equation (4) gives $R_{min} \propto h_{sp}^{0.79}$. Considering the significant data scatter around the $\log(R_{min})$ - $\log(h_{sp})$ regression, this is a reasonable match to the power law exponent computed directly from the curvature results (Figure S3a: 0.81), which suggests that the viscous subducting plates satisfy the above energy balance. However, as discussed previously and shown in Figure 3a, there does not appear to be a positive correlation between h_{sp} and R_{min} on Earth [Buffett and Heuret, 2011; Fourel et al., 2014].

Plasticity reduces the absolute value of R_{min} , relative to that of the viscous SPs. The effective viscosity of the bending region is reduced in viscoplastic SPs, and so this observation of reduced R_{min} can be understood by previous work [Bellahsen et al., 2005; Di Giuseppe et al., 2008; Schellart, 2008, 2009; Capitanio et al., 2009] which demonstrates that viscous SPs with reduced bulk η' have reduced R_{min} . This is in-line with the suggestion of Capitanio et al. [2007, 2009] that bending dissipation is controlled by the magnitude of slab pull, with R adjusting to produce a particular bending dissipation which is independent of SP rheology.

A plastic viscosity component also significantly reduces the strength of the dependence of R_{min} on h_{sp} (Figure 2b), more in-line with the apparent absence of a positive trend on Earth. If one assumes a similar proportionality between buoyancy flux and bending dissipation for a plastic plate with constant yield stress, then $R_{min} \propto h_{sp}$ is expected [Buffett, 2006]. Since the observed relationship is not linear (Figure 2b), the assumption that bending dissipation is a constant fraction of the buoyancy flux is likely violated. While the inclusion of a laboratory-derived composite rheology with pressure-dependent yielding may improve the agreement between observations and model systematics, we use our simplified modeling approach to propose that weakening of the SP bending region is an important component in diminishing the positive correlation between R_{min} and h_{sp} expected for viscous SPs. For a plastic SP, the bending stresses in the hinge can become insufficient to balance the torque due to buoyancy [Buffett and Becker, 2012]. Thus, Buffett and Becker [2012] propose that forces on the surface of the slab, potentially associated with the low-viscosity crustal channel and/or the mantle wedge, must play an essential role in balancing the gravitational torque.

5.2. Curvature as a Function of OP Thickness

We find that the overriding plate thickness, h_{op} , plays indeed a significant role in dictating SP curvature. As h_{op} increases, the length of the plate interface, composed of weak "crustal" material, increases. This weak channel, as well as the adjacent portion of the OP/mantle wedge, is under low dynamic pressure (Figure S4), which prevents the SP from detaching from the OP. For large h_{op} , this prohibits the curvature, R_{min} , from reducing significantly below that initially imposed (R_{init}). On the other hand, because the OP is relatively strong and contains no rheological weakening, R_{min} cannot increase above R_{init} for thick OPs, as this requires deforming the OP. Therefore, for $h_{op} = 125$ km, all SP rheologies result in comparable R_{min} . On Earth, this is analogous to the initial geometry of a subduction zone interface/thrust controlling the subsequent curvature evolution for thick OPs, as initially proposed by Jarrard [1986].

While R_{min} is strongly affected by R_{init} for thick OPs, this is not the case for thin OPs. As h_{op} is reduced, the plate interface control reduces, and slab curvature tends toward the single-plate R_{min} (i.e., without OP influence). For viscoplastic models, as discussed in the previous section, slabs have a naturally reduced R_{min} relative to the isoviscous SPs. Thus, plastic models have reduced curvature for low h_{op} which, because R_{min} is relatively constant between different rheologies for high h_{op} , results in a strong positive trend between R_{min} and h_{op} , relative to that observed for isoviscous SPs. The strength of this trend is dependent on the interface geometry initially imposed, R_{init} (Figure S5). Viscoplastic models with a lower R_{init} of 200 km have a weaker positive trend because R_{min} is reduced for the high h_{op} values, where it is strongly influenced by the plate interface geometry and only slightly modified for low h_{op} (25 km). However, for all R_{init} explored (200 km to 300 km), the positive

trend is always stronger in models with viscoplastic SPs relative to purely viscous SPs (Figure S5). In addition, an R_{init} of 300 km is required to produce a positive $h_{\text{OP}}-R_{\text{min}}$ trend for the viscous SP models, which is significantly greater than the average R_{min} of ≈ 200 km estimated for Earth [Buffett and Heuret, 2011].

We infer a positive trend between h_{OP} and R_{min} in natural subduction zones (Figure 3b). Informed by the modeling work, we suggest that this is due to a combination SP hinge weakening [e.g., Ranero et al., 2003, 2005], and the preexisting geometry of the plate interface [e.g., Jarrard, 1986]. Due to the large uncertainty inherent in estimating lithospheric thickness from global tomographic models [e.g., Fischer et al., 2010], the data compilation serves only to investigate the first-order nature of the relationship between h_{OP} and R_{min} on Earth, and so we have not attempted to interpret the specific functional form of the regression (Figure 3b). In addition, we expect contributions from other OP mechanical properties that are coupled to h_{OP} , such as the OP density which exerts a control on the lithostatic pressure gradient between the two plates. However, the correlation of R_{min} and h_{OP} is significantly stronger than that observed between R_{min} and h_{SP} . It therefore appears that the OP structure is playing a key role in dictating curvature of the SP, which is compatible with the positive correlation between R_{min} and h_{OP} observed only for viscoplastic SPs (Figure 2a).

6. Conclusions

We used numerical subduction models to investigate how the addition of a plastic rheology component modifies the dependence of subducting plate curvature (R_{min}) on subducting and overriding plate thickness (h_{SP} and h_{OP}), relative to the systematics observed for the isoviscous SPs typically considered. Plasticity is found to reduce the strength of the positive correlation between h_{SP} and R_{min} and increase the strength of the positive trend between R_{min} and h_{OP} . Such a positive trend, between R_{min} and h_{OP} , appears to be present on Earth. We therefore suggest that the structure of the overriding plate, and plastic weakening of the bending region of the subducting slab, are integral components in dictating subducting slab curvature on Earth. In addition to being a key control on the amount of energy dissipated during plate bending, the evolution of slab curvature has possible implications for long-term force transmission on subduction zone interfaces.

Acknowledgments

We thank Serge Lallemand and Jeroen van Hunen for constructive comments which helped improve the manuscript, and the original authors and CIG (geodynamics.org) for providing CitcomCU. Computations were performed on USC's High Performance Computing Center, and all plots were made with the Generic Mapping Tools [Wessel et al., 2013]. All data sets and software used are available upon request.

The Editor thanks Serge Lallemand and Jeroen van Hunen for their assistance in evaluating this paper.

References

- Becker, T. W., C. Faccenna, R. J. O'Connell, and D. Giardini (1999), The development of slabs in the upper mantle: Insights from experimental and laboratory experiments, *J. Geophys. Res.*, *104*, 15,207–15,226.
- Běhounková, M., and H. Čížková (2008), Long-wavelength character of subducted slabs in the lower mantle, *Earth Planet. Sci. Lett.*, *275*, 43–53, doi:10.1016/j.epsl.2008.07.059.
- Bellahsen, N., C. Faccenna, and F. Funiciello (2005), Dynamics of subduction and plate motion in laboratory experiments: Insights into the "plate tectonics" behavior of the Earth, *J. Geophys. Res.*, *110*, B01401, doi:10.1029/2004JB002999.
- Billen, M. I., and M. Gurnis (2001), A low viscosity wedge in subduction zones, *Earth Planet. Sci. Lett.*, *193*, 227–236.
- Bird, P., Z. Liu, and W. K. Rucker (2008), Stresses that drive the plates from below: Definitions, computational path, model optimization, and error analysis, *J. Geophys. Res.*, *113*, B11406, doi:10.1029/2007JB005460.
- Buffett, B. A. (2006), Plate force due to bending at subduction zones, *J. Geophys. Res.*, *111*, B09405, doi:10.1029/2006JB004295.
- Buffett, B. A., and T. W. Becker (2012), Bending stress and dissipation in subducted lithosphere, *J. Geophys. Res.*, *117*, B05413, doi:10.1029/2012JB009205.
- Buffett, B. A., and A. Heuret (2011), Curvature of subducted lithosphere from earthquake locations in the Wadati-Benioff zone, *Geochem. Geophys. Geosyst.*, *12*, Q06010, doi:10.1029/2011GC003570.
- Capitanio, F. A., G. Morra, and S. Goes (2007), Dynamic models of downgoing plate-buoyancy driven subduction: Subduction motions and energy dissipation, *Earth Planet. Sci. Lett.*, *262*, 284–297, doi:10.1016/j.epsl.2007.07.039.
- Capitanio, F. A., G. Morra, and S. Goes (2009), Dynamics of plate bending at the trench and slab-plate coupling, *Geochem. Geophys. Geosyst.*, *10*, Q04002, doi:10.1029/2008GC002348.
- Conrad, C., and B. Hager (1999), Effects of plate bending and fault strength at subduction zones on plate dynamics, *J. Geophys. Res.*, *104*, 17,551–17,571.
- Di Giuseppe, E., J. van Hunen, F. Funiciello, C. Faccenna, and D. Giardini (2008), Slab stiffness control of trench motion: Insights from numerical models, *Geochem. Geophys. Geosyst.*, *9*, Q02014, doi:10.1029/2007GC001776.
- Enns, A., T. W. Becker, and H. Schmeling (2005), The dynamics of subduction and trench migration for viscosity stratification, *Geophys. J. Int.*, *160*, 761–775.
- Fischer, K. M., H. A. Ford, D. L. Abt, and C. A. Rychert (2010), The lithosphere-asthenosphere boundary, *Ann. Rev. Earth Planet. Sci.*, *38*, 551–575, doi:10.1146/annurev-earth-040809-152438.
- Forsyth, D., and S. Uyeda (1975), On the relative importance of the driving forces of plate motion, *Geophys. J. R. Astron. Soc.*, *43*, 163–200.
- Fouré, L., S. Goes, and G. Morra (2014), The role of elasticity in slab bending, *Geochem. Geophys. Geosyst.*, *15*, 4507–4525, doi:10.1002/2014GC005535.
- Frank-Kamenetskii, D. A. (1969), *Diffusion and Heat Transfer in Chemical Kinetics*, Plenum, New York.
- Funiciello, F., C. Faccenna, D. Giardini, and K. Regenauer-Lieb (2003), Dynamics of retreating slabs: 2. Insights from three-dimensional laboratory experiments, *J. Geophys. Res.*, *108*(B4), 2207, doi:10.1029/2001JB000896.
- Garel, F., S. Goes, D. R. Davies, J. H. Davies, S. C. Kramer, and C. R. Wilson (2014), Interaction of subducted slabs with the mantle transition-zone: A regime diagram from 2-D thermo-mechanical models with a mobile trench and an overriding plate, *Geochem. Geophys. Geosyst.*, *15*, 1739–1765, doi:10.1002/2014GC005257.

- Goetze, C., and B. Evans (1979), Stress and temperature in the bending lithosphere as constrained by experimental rock mechanics, *Geophys. J. R. Astron. Soc.*, *59*, 463–478.
- Heuret, A., F. Funicello, C. Faccenna, and S. Lallemand (2007), Plate kinematics, slab shape, and back-arc stress: A comparison between laboratory models and current subduction zones, *Earth Planet. Sci. Lett.*, *256*, 473–483, doi:10.1016/j.epsl.2007.02.004.
- Holt, A. F., T. W. Becker, and B. A. Buffett (2015), Trench migration and overriding plate stress in dynamic subduction models, *Geophys. J. Int.*, *201*, 172–192, doi:10.1093/gji/ggv011.
- Irvine, D. N., and W. P. Schellart (2012), Effect of plate thickness on bending radius and energy dissipation at the subduction zone hinge, *J. Geophys. Res.*, *117*, B06405, doi:10.1029/2011JB009113.
- Jarrard, R. D. (1986), Relations among subduction parameters, *Rev. of Geophys.*, *24*, 217–284.
- Karato, S., and P. Wu (1993), Rheology of the upper mantle: A synthesis, *Science*, *260*, 771–778, doi:10.1126/science.260.5109.771.
- Kincaid, C., and R. W. Griffiths (2003), Laboratory models of the thermal evolution of the mantle during rollback subduction, *Nature*, *245*, 58–62, doi:10.1038/nature01923.
- Kohlstedt, D. L., B. Evans, and S. J. Mackwell (1995), Strength of the lithosphere: Constraints imposed by laboratory experiments, *J. Geophys. Res.*, *100*, 17,587–17,602.
- Lallemand, S., and A. Heuret (2005), On the relationships between slab dip, back-arc stress, upper plate absolute motion, and crustal nature in subduction zones, *Geochem. Geophys. Geosyst.*, *6*, Q09006, doi:10.1029/2005GC000917.
- McBride, J. H., and D. E. Karig (1987), Crustal structure of the outer Banda arc: New free-air gravity evidence, *Tectonophysics*, *140*, 265–273, doi:10.1016/0040-1951(87)90234-4.
- Mei, S., A. M. Suzuki, D. L. Kohlstedt, N. A. Dixon, and W. B. Durham (2010), Experimental constraints on the strength of lithospheric mantle, *J. Geophys. Res.*, *115*, B08204, doi:10.1029/2009JB006873.
- Moresi, L. N., and M. Gurnis (1996), Constraints on the lateral strength of slabs from three-dimensional dynamic flow models, *Earth Planet. Sci. Lett.*, *138*, 15–28, doi:10.1016/0012-821X(95)00221-W.
- Ranero, C. R., J. P. Morgan, K. McIntosh, and C. Reichert (2003), Bending-related faulting and mantle serpentinization at the Middle America trench, *Nature*, *425*, 367–373, doi:10.1038/nature01961.
- Ranero, C. R., A. Villasenor, J. P. Morgan, and W. Weinrebe (2005), Relationship between bend-faulting at trenches and intermediate-depth seismicity, *Geochem. Geophys. Geosyst.*, *6*, Q12002, doi:10.1029/2005GC000997.
- Ribe, N. M. (2010), Bending mechanics and mode selection in free subduction: A thin-sheet analysis, *Geophys. J. Int.*, *180*, 559–576, doi:10.1111/j.1365-246X.2009.04460.x.
- Ritsema, J., H. J. van Heijst, and J. H. Woodhouse (2004), Global transition zone tomography, *J. Geophys. Res.*, *109*, B02302, doi:10.1029/2003JB002610.
- Schellart, W. P. (2008), Kinematics and flow patterns in deep mantle and upper mantle subduction models: Influence of the mantle depth and slab to mantle viscosity ratio, *Geochem. Geophys. Geosyst.*, *9*, Q03014, doi:10.1029/2007GC001656.
- Schellart, W. P. (2009), Evolution of the slab bending radius and the bending dissipation in three-dimensional subduction models with a variable slab to upper mantle viscosity ratio, *Earth Planet. Sci. Lett.*, *288*, 309–319, doi:10.1016/j.epsl.2009.09.034.
- Schott, B., and H. Schmeling (1998), Delamination and detachment of a lithospheric root, *Tectonophysics*, *296*, 225–247, doi:10.1016/S0040-1951(98)00154-1.
- Sharples, W., M. A. Jadamec, L. N. Moresi, and F. A. Capitanio (2014), Overriding plate controls on subduction evolution, *J. Geophys. Res. Solid Earth*, *119*, 6684–6704, doi:10.1002/2014JB011163.
- Stegman, D. R., R. Farrington, F. A. Capitanio, and W. P. Schellart (2010), A regime diagram for subduction styles from 3-D numerical models of free subduction, *Tectonophysics*, *483*, 29–45, doi:10.1016/j.tecto.2009.08.041.
- Wessel, P., W. H. F. Smith, R. Scharroo, J. Luis, and F. Wobbe (2013), Generic mapping tools: Improved version released, *Eos Trans. AGU*, *94*, 409–410, doi:10.1002/2013EO450001.
- Wu, B., C. P. Conrad, A. Heuret, C. Lithgow-Bertelloni, and S. Lallemand (2008), Reconciling strong slab pull and weak plate bending: The plate constraint on the strength of mantle slabs, *Earth Planet. Sci. Lett.*, *272*, 412–421, doi:10.1016/j.epsl.2008.05.009.
- Yamato, P., L. Husson, J. Braun, C. Loiselet, and C. Thieulot (2009), Influence of surrounding plates on 3D subduction dynamics, *Geophys. Res. Lett.*, *36*, L07303, doi:10.1029/2008GL036942.
- Zhong, S. (2006), Constraints on thermochemical convection of the mantle from plume heat flux, plume excess temperature and upper mantle temperature, *J. Geophys. Res.*, *111*, B04409, doi:10.1029/2005JB003972.